Dynamics Affecting the Primary Charge Transfer in Photosynthesis

John N. Gehlen, Massimo Marchi,* David Chandler†

Analysis of a 60-picosecond molecular dynamics trajectory of the reaction center of *Rhodopseudomonas viridis* provides an understanding of observations concerning vibrational coherence and the nonexponential kinetics of the primary charge transfer in photosynthesis. Complex kinetics arises from energy gap correlations that persist beyond 1 picosecond.

Recent observations of nonexponential relaxation in photosynthetic reaction centers (*1–4*) have spurred speculation about the mechanism of the primary charge transfer in photosynthesis. Here, we use the results of our recent molecular dynamics simulation of *Rps. viridis* (*5*) to address issues raised by these observations and suggest the source of the nonexponential kinetics of the primary charge transfer. In particular, we show that observed nonexponential kinetics of the primary electron transfer can be due to slow components of the energy gap fluctuations. These components are correlated beyond 1 ps and are significant contributors to the reorganization energy. We also identify underdamped vibrational motions with periods near 2 ps that seem to explain experimental observations of coherence. These motions are interchromophore distance fluctuations. They seem of little consequence to the electron transfer process, however, as they are weakly correlated with energy gap fluctuations and their amplitudes are small.

In the primary charge transfer, an electronic charge moves from the photoexcited special pair, SP*, to a bacteriopheophytin, BPL. In part, there is much interest in an accessory bacteriochlorophyll, BCL. The centers of SP* and BPL lie nearly 20 Å apart, and the BCL sits in between, making van der Waals contact with both chromophores. As such, it might, for example, provide a resolvable intermediate location for the transferring electron. In that case, the observed nonexponential decay of the initial photoexcited state could simply manifest two-step kinetics. A result of our modeling of the reaction center (*5*), however, is that the reduced accessory bacteriochlorophyll state, SP$^+$BCL$^-$, lies at a relatively high energy. With this arrangement of states, the intermediate state is not resolvable; it is accessed through virtual transitions. In other words, the electron transfer occurs through a "super exchange" mechanism. If this prediction is correct, the origin of the nonexponential decay requires explanation.

Nonexponential relaxation of the photoexcited state can arise in a super exchange process through an interplay between nuclear motions (or inhomogeneity) and electron transfer kinetics. A dynamical interplay is conceivable because the primary electron transfer occurs in ~10 ps or less. The transfer is thus faster than what might be the typical relaxation times of relevant nuclear motions in the reaction center. Such dynamics of the energy gap fluctuations, ε, does occur in our simulated room temperature proteic complex.

The energy gap is the difference between the electronic energies of the photoexcited state SP* and the reduced pheophytin state SP$^+$BPL$^-$. As the atoms move, electric potential fields change and the energy gap fluctuates as a result. Electron transfer between the SP* pair and the BPL occurs when that energy gap is essentially zero. That is, the transition state surface is at configurations for which the collective variable $\varepsilon = \varepsilon^*$, where ε^* denotes the average energy gap. In the simulation, the gap is computed as a function of time from the trajectories of the nitrogen atoms in the chromophores (*6*) according to specified charge distributions and scaling (*5*). The logarithm of the distribution of ε yields the diabatic free energies (Fig. 1).

Several approximations and assumptions are used in the modeling that yields these pictured diabatic surfaces. The most significant of these are (i) the use of semiempirical quantum chemical estimates (*7*) for ionization potentials and electron affinities; (ii) the use of standard pK_a values (negative logarithm of the acid constant) to fix the charges of amino acids; (iii) the accounting of electronic polarization through the reduction of average electrostatic energies and reorganization energies by the optical dielectric constant, ϵ_∞; (iv) the neglect of all other manifestations of electronic polarization as well as the neglect of the aqueous solution and membrane that surround the proteic system; and (v) the truncation of the molecular dynamics to a finite region of space and to a finite length of time. The energies obtained from quantum chemistry are in reasonable agreement with alternative estimates (*8*) and are similar for states 2 and 3. Hence, the relative positioning of the three states is due primarily to the electrostatic field created by the proteic environment. Because approximations (ii) through (iv) above are each questionable, our positioning of the diabatic surfaces must therefore involve some degree of uncertainty.

Least uncertain is the juxtaposition of states 1 and 3. The thermodynamic driving force is known from experiment; specifically, the free energy difference between states 1 and 3, ΔG_{13}, is ≈ -6 kcal mol^{-1} (*9*). Further, the primary charge transfer rate exhibits a relatively small temperature dependence (*10*), which suggests that the intersection of states 1 and 3 is nearly activationless. Both of these features are captured by the modeling with a physically reasonable value for ϵ_∞ of 1.9. Because the driving force and intersection are apparently correct, the modeling seems to produce a realistic curvature for the surfaces and, consequently, a realistic reorganization energy. Therefore, although the location of state 2 may remain in question (*8*), the modeling

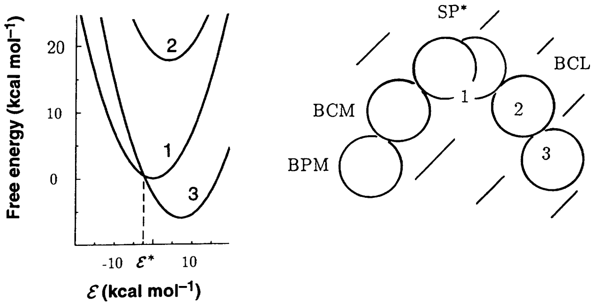

Fig. 1. Free energies of the L branch of *Rps. viridis* as functions of ε, the fluctuation in the energy gap between states 1 and 3 as computed in (*5*). State 1 is the photoexcited special pair, SP*; state 2 is the charge-separated state SP$^+$BCL$^-$ where the transferring electron resides on the accessory bacteriochlorophyll, BCL; and state 3 is SP$^+$BPL$^-$, where the electron has been transferred to the bacteriopheophytin. A schematic of the central chromophores, indicating the spatial arrangement of the charge-localized states, is shown at the right. The corresponding calculated free energies for the inactive M branch show that the reaction SP* → SP$^+$BPM$^-$ is endothermic, with a significant activation barrier (*5*).

Department of Chemistry, University of California, Berkeley, CA 94720.

*Present address: Section de Biophysique des Proteines et des Membranes, Departement de Biologie Cellulaire et Moléculaire, Centre d'Études de Saclay, 91191 Gif-Sur-Yvette, France
†To whom correspondence should be addressed.

appears sufficiently realistic to treat the kinetics of the primary charge transfer if indeed that process occurs through super exchange.

Figure 2 provides a dynamical perspective of the nearly activationless intersection of states 1 and 3. Throughout the illustrated 60-ps period, the energy gap remains close to its transition state, crossing it many times, at a rate of typically 10 ps^{-1}. The frequency of crossings remains relatively constant for stretches of 5 to 10 ps. From one stretch to the next, however, the frequency of crossings increases or decreases by factors of ~3. In other words, the low-frequency motions of the energy gap mediate the high frequency of crossings. The cumulative number of crossings, $N(t)$, is illustrated at the bottom of Fig. 2. Three different functions are shown to indicate a range of uncertainty in $N(t)$ that is attributable to uncertainty in ε^* (*11*).

A surface hopping model where

$$S(t) = \langle (1 - p)^{N(t)} \rangle \qquad (1)$$

provides a means to predict the effects of this pictured dynamics on the primary electron transfer kinetics. Here, $S(t)$ stands for the survival probability of the photoexcited state, the indicated average is an equilibrium average over trajectories initiated in the photoexcited state, and p is the probability that the electron transfer will occur given that $\varepsilon = \varepsilon^*$. On average, and for long enough times, $N(t)$ is extensive in time. If $pN(t)/t$ were generally small compared to energy gap relaxation rates, there would be little correlation between one electronic transition and the next and $N(t)$ would be effectively linear for all relevant times. In that case

$$S(t) \approx e^{-kt} \qquad (2)$$

where

$$k = p\langle N(t)\rangle/t \approx (2\pi/\hbar)K_{\mathrm{eff}}^2 \langle \delta(\varepsilon - \varepsilon^*)\rangle \qquad (3)$$

The approximate equality in Eq. 3 follows from a Landau-Zener estimate for p, where $K_{\mathrm{eff}} = \overline{H}^2/\Delta E$ is the effective electronic coupling between the states SP* and $\mathrm{SP^+BPL^-}$ and $\hbar$ is Planck's constant divided by 2π (*12*) [$\overline{H}$ refers to the geometric mean of the (nearest neighbor) electronic couplings between states 1 and 2 and 2 and 3 and ΔE is the virtual gap—that is, the average energy difference between states 1 and 2 at the configurations where states 1 and 3 intersect]. Equations 2 and 3 coincide with the standard "golden rule" expression for the rate of electron transfer k (*12*). From the observed decay of the photoexcited state, we anticipate $k \sim 0.2\ \mathrm{ps}^{-1}$. On the time scale set by this rate constant, however, $N(t)$ is not linear in time. Hence, subsequent electronic transitions are not uncorrelated and $S(t)$ cannot decay as a single exponential.

A better approximation to what is shown in Fig. 2 is a stochastic model where the system moves at random between two regions, one for which $-N(t)\ln(1 - p)$ has slope k_1 and the other for which $-N(t)\ln(1 - p)$ has slope k_2. In the simplest case, the changes in slope occur as Markovian processes with average interconversion frequency ν. A method with which this model is analyzed analytically is described in (*13*). It yields

$$S(t) = \chi_+ e^{-\kappa_+ t} + \chi_- e^{-\kappa_- t} \qquad (4)$$

where the modulated decay constants are

$$\kappa_\pm = \frac{1}{2}\{k_1 + k_2 + \nu \pm [(k_1 + k_2 - \nu)^2 - 4(k_1k_2 - \nu\Delta k)]^{1/2}\} \qquad (5)$$

and

$$\chi_\pm = \pm(\kappa_\pm + \nu + \Delta k)/(\kappa_+ - \kappa_-) \qquad (6)$$

Here, $\Delta k = x_2k_1 + x_1k_2$, where $x_1 = 1 - x_2$ is the fraction of time where $-N(t)\ln(1 - p)$ has slope k_1. Note that Eq. 4 is the inverse Laplace transform of $\tilde{S}(z) = \tilde{S}_0(z + \nu)/[1 - \nu\tilde{S}_0(z + \nu)]$, where $\tilde{S}_0(z)$ is the Laplace transform of the inhomogeneous decay function

$$S_0(t) = x_1\exp(-k_1t) + x_2\exp(-k_2t) \qquad (7)$$

As ν becomes large compared to k_1 or k_2, $S(t)$ tends to $\exp(-\bar{k}t)$, where $\bar{k} = k_1x_1 + k_2x_2$. Corrections are of order ν^{-2} and involve a quickly decaying exponential, $\exp(-\nu t)$. In the opposite limit, $\nu \rightarrow 0$, $S(t)$ becomes $S_0(t)$.

The parameterizations relevant to the reaction center lie between these fast- and slow-exchange regimes. Judging from Fig. 2, k_1/k_2 is in the vicinity of 3, ν should be ~0.1 to 0.2 ps^{-1}, and x_1 is ~0.5. Figure 3 shows a comparison of Eq. 4 with experimental results for this range of parameters, restricting k_1/k_2 to 3. The root-mean-square (rms) deviation of the fit of the stochastic

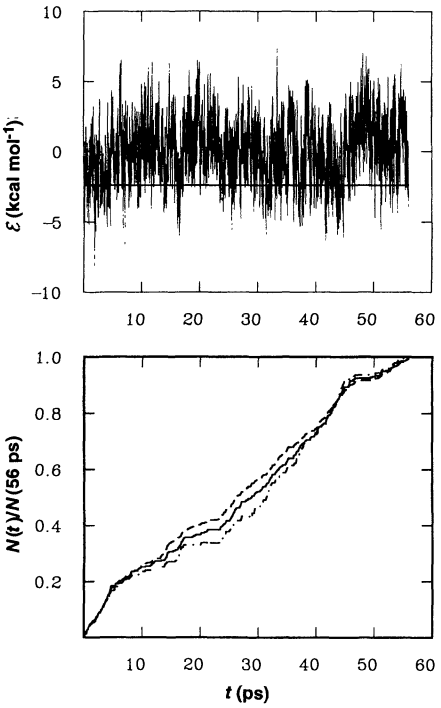

Fig. 2. Primary charge transfer energy gap fluctuations, $\varepsilon(t)$, and the cumulative number of $\varepsilon(t) = \varepsilon^*$ crossings, $N(t)$. The estimate of $\varepsilon^* = -2.4$ kcal mol^{-1} is shown as the horizontal line in the upper graph. The corresponding value for $N(t)$ is pictured with the solid line, and N(56 ps) = 648 for that case. The dashed and dashed-dotted lines in the bottom graph show values for $N(t)$ for the cases with $\varepsilon^* = -1.9$ and -2.9 kcal mol^{-1}, respectively and with the corresponding values of N(56 ps) = 804 and 512, respectively.

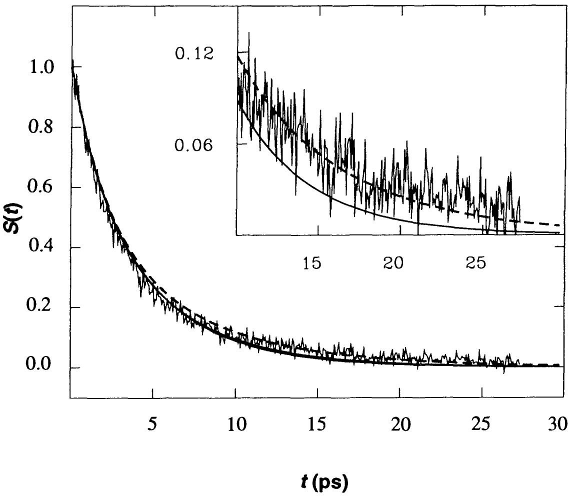

Fig. 3. Survival probability, $S(t)$. The jagged line is the experimental data of Du *et al.* (*2*). The solid line represents two different fits to the data (indistinguishable on the scale of the lower graph) with Eq. 4 with the use of either (i) $\nu^{-1} = 5$ ps with $x_1 = 0.52$, $k_1^{-1} = 2.3$ ps, and $k_2^{-1} = 6.8$ ps or (ii) $\nu^{-1} = 10$ ps with $x_1 = 0.57$, $k_1^{-1} = 2.4$ ps, and $k_2^{-1} = 7.1$ ps. The dashed line represents (i) but is treated in the inhomogeneous approximation—that is, $\nu = 0$. The insert (upper right) expands the scale for comparison of (i) with the inhomogeneous approximation for $t \geq 10$ ps. Values of k_1 and k_2 in the range of 1 to 0.1 ps^{-1} coincide with $\overline{H} \approx 300\ \mathrm{cm}^{-1}$ as $\Delta E \approx 20$ kcal mol^{-1} in the simulation model (*5*). The corresponding hopping probability, $p \approx 2\pi K_{\mathrm{eff}}^2/\hbar\langle|\dot{\varepsilon}|\rangle$ is $\sim 10^{-2}$ as $\langle|\dot{\varepsilon}|\rangle \approx 115$ kcal $\mathrm{mol}^{-1}\ \mathrm{ps}^{-1}$ in the simulation model.

model to the data of Du *et al.* (*2*) is $\sim 1.7 \times 10^{-2}$. However, smaller deviations can be obtained by allowing k_1/k_2 to be as large as 5. Although not observed during our simulation run, such a large change in slope is conceivable in view of our limited statistics. Even with our limited statistics, however, the plot in Fig. 3 shows that the observed nonexponential decay can be satisfactorily explained as a consequence of the post picosecond motions found in the simulation model.

The stochastic model that underlies Eq. 4 can be used to predict the required trajectory length for accurately computing $S(t)$ directly from a molecular dynamics run. In particular, one can generate a long but finite trajectory for $N(t)$ from the Poisson distribution with interconversion frequency ν. Averaging over this trajectory yields an estimate of $S(t)$ that can be compared with the exact analytical result for the model (Eqs. 4 to 6). With $\nu \approx 0.1$ ps^{-1} and $k_1/3 \approx k_2 \approx 0.1$ ps^{-1}, for example, the finite time averaging calculation of $S(t)$ with $0 < t < 10$ ps incurs errors <0.03, provided the length of the trajectory exceeds 2×10^3 ps. Therefore, a straightforward interpretation of the primary electron transfer kinetics from molecular dynamics models requires trajectories >1 ns in duration. Inferences drawn from shorter runs, such as ours, require some extra degree of modeling.

For the pertinent range of parameters, the difference between the dynamical model and the inhomogeneous approximation, $S_0(t)$, is not large. A comparison is illustrated in Fig. 3. Qualitatively, therefore, one may view the nonexponential decay as the result of a statistical distribution of thermodynamic driving forces. This picture has been advanced by Fleming and Norris and their co-workers (*2*, *14*, *15*). To be consistent with our simulation results, the distribution of driving forces cannot coincide with a variety of static environments for the chromophores, as in a glassy system. In contrast with a glassy variable that could relax into a multitude of potential minima, our simulation indicates that the dynamics of the primary transfer energy gap is reasonably linear with a harmonic monostable potential surface (*5*). As such, the statistics of the gap are essentially Gaussian. One can divide the energy gap fluctuations into contributions from different frequency components, and the statistics of each of these components is Gaussian. Fluctuations of slow energy gap components in a linear-responding model may be viewed equivalently in terms of a Gaussian distribution of driving forces for the faster fluctuations.

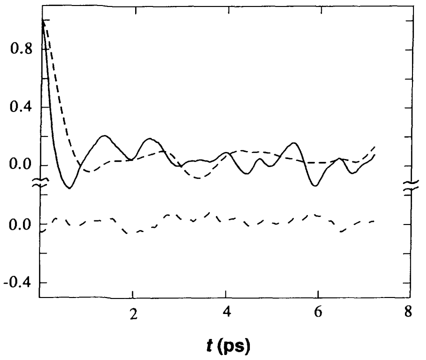

Fig. 4. Correlation functions for fluctuations in separation between chromophore centers. The solid line is $\langle \delta r(t) \delta r(0) \rangle / \langle (\delta r)^2 \rangle$ where $r(t)$ is the distance between the SP bacteriochlorophylls, SPL-SPM; in this case, $\langle (\delta r)^2 \rangle^{1/2} = 0.14$ Å. The dashed line is the corresponding function for the distance between the center of SPM and the center of the accessory bacteriochlorophyll, BCL; in this case, $\langle (\delta r)^2 \rangle^{1/2} = 0.15$ Å. The dashed-dotted line, shown on the offset plot with the same vertical scale, is the cross-correlation function $\langle \delta r(t) \delta \varepsilon(0) \rangle / \langle (\delta r)^2 \rangle^{1/2} \langle \varepsilon^2 \rangle^{1/2}$ where $r(t)$ is the SPL-SPM separation.

Decomposed into its Fourier components, $\hat{\varepsilon}(\omega)$, the statistics of $\varepsilon(t)$ is characterized by $\langle |\hat{\varepsilon}(\omega)|^2 \rangle$. The integrated area of this spectral density is proportional to the reorganization energy. The spectral density of the simulation model (*5*) is broad and nearly featureless, as expected for a heteropolymer system. In the parlance of quantum dissipative systems, it coincides with "ohmic" dissipation (*16*). We find $\langle |\hat{\varepsilon}(\omega)|^2 \rangle$ is largest at zero frequency and decays nearly monotonically with 80% of its intensity in the range $\omega/2\pi \lesssim 10$ ps^{-1} (corresponding to $\omega \lesssim 400$ cm^{-1}). Slow fluctuations—that is, those with $\omega/2\pi \lesssim 1$ ps^{-1}—contribute 40% of the total reorganization energy of the model. Earlier simulation work (*17*) did not reveal nor consider the possibility of correlations in ε beyond 1 ps.

In addition to the low-frequency components of ε, there are many other postpicosecond correlations in the reaction center, some of which could be pertinent to the primary charge transfer. Consider, for example, the distances separating neighboring chromophore rings. The spatial arrangement of the central chromophores affects the nearest neighbor electronic coupling. Fluctuations in these configurations could therefore mediate the transfer kinetics. Figure 4 shows the correlation functions for some of the interring distances in the reaction center. Most interesting are the underdamped oscillations of period near 2 ps. As the separation between the two bacteriochlorophylls in the SP affects the dipole of SP and SP*, it is plausible that these 2-ps oscillations coincide with the dynamics that has been observed by Vos *et al.* (*1*).

The amplitude of the interring distance fluctuations are, however, very small; from the simulation, we find rms values of 0.15 Å or less. A fluctuation in separation, δr, has a corresponding relative change in electron transfer rate:

$$\delta k/k \approx (d \ln k/dr)\delta r \qquad (8)$$

As $-d \ln k/dr \equiv \beta$ is typically about 1 Å^{-1} (*18*), the interring motions likely lead to fluctuations in rate no larger than 15%—too small to satisfactorily explain the observed transfer kinetics. We have also examined fluctuations in the relative orientations of neighboring chromophores. The associated correlation functions exhibit the 2-ps underdamped motion as well as much higher frequency components, but here too the amplitude of these fluctuations ($\delta\theta \lesssim 5°$) seems too small to have a qualitative effect on the transfer kinetics (*19*).

It is perhaps conceivable that a detailed theoretical analysis of the interring electronic couplings will reveal sensitivities to interring separations far greater than those we cite from current experimental estimates. A large enough sensitivity would imply that the interring motions could affect the electron transfer kinetics and provide a second or alternative explanation of the observed nonexponential relaxation. Indeed, we speculated (*5*) that such motions do cause the complex kinetics. In view of our current analysis, however, this mechanism seems less likely than that associated with slow energy gap fluctuations.

It is interesting that the interring motions seem to have little correlation with the primary energy gap fluctuations. In particular, from the simulation model we have computed the cross correlation $\langle \delta\varepsilon(0)\delta r(t) \rangle$. We find it to be insignificant, no larger than 10% of $(\langle \delta\varepsilon^2 \rangle \langle \delta r^2 \rangle)^{1/2}$ (Fig. 4). This result may mitigate possible concerns that the computed time dependence $\delta r(t)$ manifests significant artifacts that are a result of boundary effects in the simulation. Artificial boundary conditions imposed as a computational expedient can, in some systems, lead to periodic echoes in the molecular dynamics. Were this the case in the current system, one would expect to observe correlated periodic motions between $\varepsilon(t)$ and $\delta r(t)$.

In the super exchange mechanism, where the effective coupling between states 1 and 3 is $\overline{H}^2/\Delta E$, changes in rate could also be affected by fluctuations in the virtual energy gap, ΔE. The size of typical energy gap fluctuations is 2 kcal mol^{-1}, as gleaned from Fig. 2 or from the reorganization energy computed from the simulation model (*5*). This size is only 10% of the average virtual gap. As such, this type of fluctuation would not provide an explanation of the observed nonexponential kinetics. This conclusion, as well as our observation of no pertinent gross heterogeneity, are consistent with the observations of Small and co-workers (*20*).

The simulation model previously described (*5*) has allowed us to examine various possible explanations for the observed nonexponential charge transfer kinetics in photosynthesis. Most important are correlations in the energy gap that persist beyond 1 ps. The underlying motions are slow enough so that their effects on the charge transfer can be viewed qualitatively in terms of a statistical distribution of thermodynamic driving forces. The distinction between a statistical model and a dynamical treatment can be of importance, however, for quantitative issues. The temperature dependence of the charge transfer kinetics may be one such issue. Lowering temperature will likely increase k_1 and decrease k_2 (because these slopes specify rates for essentially activationless and slightly activated crossings, respectively). Lowering temperature, T, should also decrease x_1 (because the mean squared amplitude of low-frequency fluctuations scales as T). It does not necessarily follow, however, that lowering temperature will cause $S(t)$ to exhibit both a shorter time decay of decreased amplitude and a slower long-time decay of increased amplitude. The dynamically mediated constants, κ_+, κ_-, and χ_+, precisely follow the trends of k_1, k_2, and x_1 only in the statistical or inhomogeneous case (that is, with small values of ν). Outside that regime, the correspondence is not quite so simple, as is evident from Eqs. 5 and 6. The underlying surface-hopping model neglects nuclear tunneling effects that are significant at very low temperatures. Nevertheless, these equations illustrate how the temperature dependence may be more complicated than what might be conceived of from a purely statistical perspective. This particular topic is worthy of future theoretical work, both with molecular dynamics and analytical modeling.

REFERENCES AND NOTES

1. M. H. Vos *et al.*, *Proc. Natl. Acad. Sci. U.S.A.* **88**, 8885 (1991); M. H. Vos, F. Rappaport, J.-C. Lambry, J. Breton, J.-L. Martin, *Nature* **363**, 320 (1993).
2. M. Du *et al.*, *Proc. Natl. Acad. Sci. U.S.A.* **89**, 8517 (1992).
3. P. Hamm *et al.*, *Biochim. Biophys. Acta* **1142**, 99 (1993).
4. M. G. Muller, K. Griebenow, A. R. Holzwarth, *Chem. Phys. Lett.* **199**, 465 (1992).
5. M. Marchi, J. N. Gehlen, D. Chandler, M. Newton, *J. Am. Chem. Soc.* **115**, 4178 (1993).
6. For an equilibrated molecular dynamics run of 60 ps as described (*5*), the coordinates of all the nitrogens in the chromophores at the center of the reaction center were recorded every 2.4 fs. The file of these coordinates and the local electrostatic potentials, nitrogen.dat, can be accessed in the directory, rxncntr, through anonymous Internet file transfer protocol (ftp) from hydrogen.cchem.berkeley.edu.
7. M. A. Thompson and M. C. Zerner, *J. Am. Chem. Soc.* **113**, 8210 (1991).
8. W. W. Parson, Z.-T. Chu, A. Warshel, *Biochim. Biophys. Acta* **1017**, 251 (1990).
9. R. A. Goldstein, L. Takiff, S. G. Boxer, *ibid.* **934**, 253 (1988); A. Ogrodnik, M. Volk, R. Letterer, R. Feick, M. E. Michel-Beyerle, *ibid.* **936**, 361 (1988).
10. G. R. Fleming, J. L. Martin, J. Breton, *Nature* **333**, 190 (1988).
11. One may arrive at the ±0.5 kcal mol^{-1} uncertainty in ε^* from the simulation averages and statistical uncertainties (*5*), together with the experimental driving force (*9*) and a plausible range for the optical dielectric constant of the proteic system (that is, $\epsilon_\infty = 1.9 \pm 0.3$). Alternatively, this estimate of the uncertainty can be derived by following precisely the analysis described in (*5*) to compute ε^* and asserting a ±4 kcal mol^{-1} uncertainty in the vacuum redox potentials of Thompson and Zerner (*7*).
12. J. Ulstrup, *Charge Transfer in Condensed Media* (Springer-Verlag, Berlin, 1979).
13. N. G. van Kampen, *Stochastic Processes in Physics and Chemistry* (North-Holland, Amsterdam, 1981), pp. 203–208.
14. Z. Wang, R. M. Pearlstein, Y. Jia, G. R. Fleming, J. R. Norris, *Chem. Phys.* **176**, 421 (1993).
15. Y. Jia *et al.*, *J. Phys. Chem.* **97**, 13180 (1993).
16. A. J. Leggett *et al.*, *Rev. Mod. Phys.* **59**, 1 (1987); U. Weiss, *Quantum Dissipative Systems* (World Scientific, River Edge, NJ, 1993).
17. H. Treutlein *et al.*, *Proc. Natl. Acad. Sci. U.S.A.* **89**, 75 (1992).
18. C. C. Moser, J. M. Keske, K. Warncke, R. S. Farid, P. L. Dutton, *Nature* **355**, 796 (1992).
19. A. Helms, D. Heiler, G. McLendon, *J. Am. Chem. Soc.* **113**, 4325 (1991).
20. G. J. Small, J. M. Hayes, R. J. Silbey, *J. Phys. Chem.* **96**, 7499 (1992); P. A. Lyle, S. V. Kolaczkowski, G. J. Small, *ibid.* **97**, 6924 (1993).

21. Supported by NSF through an allocation at the University of California, San Diego, Super Computer Center and by the Department of Energy through support to D.C. and J.N.G. M.M. has benefited from support and encouragement from G. Ciccotti of Centre Européen de Calcul Atomique et Moleculaire. In addition, communications with G. R. Fleming and J. R. Norris have been helpful.

28 September 1993; accepted 1 December 1993

Decomposition of the Modulated Waves in a Rotating Couette System

Yasushi Takeda,* Walter E. Fischer, Jun Sakakibara

The time-dependent velocity field in a rotating Couette system has been decomposed. Successive instantaneous velocity profiles were obtained by an ultrasonic Doppler velocity profile method, and the spatiotemporal velocity field had been analyzed by two-dimensional Fourier transform. The Fourier spectrum is depicted by intrinsic peaks, and the velocity field cpan be reconstructed with these peak components only, indicating a successful decomposition of the velocity field. This method shows that the so-called broadband component, which is purely spatiotemporal and attributed to chaos, corresponds to a global motion of the wave propagating from roll to roll.

Decomposition of velocity fields in fluid flow into spatial and temporal modes of orthogonal eigenfunctions has long been a challenge in the investigation of hydrodynamic instabilities and coherent structures in turbulence. The theoretical basis has been developed as a proper orthogonal decomposition (or Karhunen-Loeve expansion) (*1, 2*), an empirical orthogonal decomposition (*3*), a singular value decomposition (*4*), and a bi-orthogonal decomposition (*5*), to name a few. These have been tested primarily with computed flow fields. There have been, however, only few applications to experimental work (*3–8*). This is mainly because of the lack of a suitable measurement method that can obtain spatial information on the velocity field with sufficient data as well as good time resolution. We have developed a method that makes use of a pulsed ultrasonic Doppler technique (*9*). This method allows us to obtain the spatiotemporal information necessary to decompose the velocity field.

We applied this method to investigate the modulated wavy state of the flow in a rotating concentric double cylinder. This configuration, a rotating Couette system, is frequently used to investigate a passage of flow transition from a laminar state to turbulence because the transition is gradual and has no hysteresis with respect to the Reynolds number (*10*). With this configuration, it was also concluded that the flow goes from a laminar to a chaotic state and eventually displays turbulence (*11*).

In a system with the outer cylinder fixed, the fluid in the annular gap moves as a sheet without an axial velocity component for small Reynolds numbers. The first flow instability sets in at a critical Reynolds number (R_c), resulting in the formation of a roll structure [Taylor vortex flow (TVF)] with a nonzero axial velocity component. The flow configuration then consists of stacked tori (rolls) of a pair of countercirculating vortices. At higher Reynolds numbers, a second instability sets in, and an azimuthal wave appears [wavy vortex flow (WVF)]. Power spectrum studies (*11–13*) of this flow indicate that WVF has a single mode and is periodic. At still higher Reynolds numbers, this azimuthal wave is mod-

---

Y. Takeda and W. E. Fischer, Paul Scherrer Institute, Villigen, Switzerland.
J. Sakakibara, Department of Mechanical Engineering, Keio University, Yokohama, Japan.

---

*To whom correspondence should be addressed.